

Study of Open Star Clusters Using the Gaia DR3: I-Poorly Studied King 2 and King 5

**A. A. Haroon^{1,2}, W. H. Elsanhoury^{3,*}, E. A. Elkholy^{2,3}, A. S. Saad^{2,4}
D. C. Çınar⁵**

¹Astronomy and Space Science Department, Faculty of Science, King Abdulaziz University, Jeddah, Kingdom of Saudi Arabia

²Astronomy Department, National Research Institute of Astronomy and Geophysics (NRIAG) 11421, Helwan, Cairo, Egypt

³Physics Department, College of Science, Northern Border University, Arar, Saudi Arabia

⁴Department of Management Information System, College of Business and Economics, Qassim University, P.O. BOX 6666, Buraidah 51452, Saudi Arabia

⁵Istanbul University, Institute of Graduate Studies in Science, Programme of Astronomy and Space Sciences, 34116, Beyazit, Istanbul, Turkey

* Author to whom any correspondence should be addressed.

E-mail: elsanhoury@nbu.edu.sa

XX XXXX (XX XX)

Abstract. In this study, we utilize photometric and kinematic data from *Gaia* DR3 and the ASTECA package to analyze the sparsely studied open clusters, King 2 and King 5. For King 2, we identify 340 probable members with membership probabilities exceeding 50%. Its mean proper motion components are determined as $(\mu_\alpha \cos \delta, \mu_\delta) = (-1.407 \pm 0.008, -0.863 \pm 0.012)$ mas yr⁻¹, and its limiting radius is derived as $6.94_{-1.06}^{+0.22}$ arcminutes based on radial density profiles. The cluster has an estimated age of 4.80 ± 0.30 Gyr, a distance of 6586 ± 164 pc, and a metallicity of $[\text{Fe}/\text{H}] = -0.25$ dex ($z = 0.0088$). We detect 17 blue straggler stars (BSSs) concentrated in its core, and its total mass is estimated to be $356 \pm 19 M_\odot$. The computed apex motion is $(A_o, D_o) = (-142^\circ 61 \pm 0^\circ 08, -63^\circ 58 \pm 0^\circ 13)$. Similarly, King 5 consists of 403 probable members with a mean proper motion components $(\mu_\alpha \cos \delta, \mu_\delta) = (-0.291 \pm 0.005, -1.256 \pm 0.005)$ mas yr⁻¹ and a limiting radius of $11.33_{-2.16}^{+5.45}$ arcminutes. The cluster's age is determined as 1.45 ± 0.10 Gyr, with a distance of 2220 ± 40 pc and a metallicity of $[\text{Fe}/\text{H}] = -0.15$ dex ($z = 0.0109$). We identify 4 centrally concentrated BSSs, and the total mass is estimated as $484 \pm 22 M_\odot$. The apex motion is calculated as $(A_o, D_o) = (-115^\circ 10 \pm 0^\circ 09, -73^\circ 16 \pm 0^\circ 12)$. The orbital analysis of King 2 and King 5 indicates nearly circular orbits, characterized by low eccentricities and minimal variation in their apogalactic and perigalactic distances. King 2 and King 5 reach maximum heights of 499 ± 25 pc and 177 ± 2 pc from the Galactic plane, respectively, confirming their classification as young stellar disc population.

Keywords: Open clusters, *Gaia* DR3, AStCA package, Color-magnitude diagrams CMDs, Kinematics.

1. Introduction

Open clusters (OCs) are fundamental probes for investigating the formation and evolution of the Milky Way. Their broad age distribution offers a timeline for studying the development of the Galactic disc, from its early formation to more advanced stages. The spatial distribution and kinematic properties of OCs provide important insights into the gravitational potential and the perturbations affecting the structure and dynamics of the Galaxy. By examining the evolutionary paths and eventual dissolution of OCs, we can better understand the processes behind the assembly and long-term evolution of the Galactic disc, as well as the formation and structure of spiral galaxies. These analyses are essential for building a comprehensive model of Galactic evolution. Most OCs dissipate completely within a few million years (Spitzer & Hart, 1971; Bhattacharya et al., 2022; Liu et al., 2025). The OCs known to be older than 1 Gyr are thought to have persisted because of their specific orbital characteristics, which help them to avoid close encounters with the Galactic plane (Friel, 1995). Several dynamical processes contribute to the eventual disruption of OCs, including internal interactions between member stars, stellar evolution, collisions with giant molecular clouds, and gravitational influences from the Galactic potential (see e.g., Gustafsson et al., 2016).

OCs play an important role in the calibration of the cosmic distance scales due to the precise determination of their distances. Their well-constrained ages and metallicities make them key benchmarks for stellar evolution models and standard candles (e.g., Gaia Collaboration et al., 2018; Bossini et al., 2019; Cantat-Gaudin et al., 2020; Gaia Collaboration et al., 2021, 2023). On the other hand, to constrain the initial luminosity functions (LF) and initial mass functions (IMF) in stellar populations. In addition, the radial velocities of OCs have been used to study local Galactic kinematics, including the motion of the Sun, the Oort constants (A & B), and the rotation curve of the Galaxy. Older clusters, especially those at larger distances, provide important data for identifying metallicity gradients within the Galactic disc, relating cluster age to metallicity, and revealing the complex history of chemical enrichment and mixing processes within the disc (Friel, 1995; Alfonso, Vieira, & Garcia-Varela, 2024).

The dynamics of OCs, which are intimately linked to their orbital properties and metallicity, provide deep insights into the processes governing their formation and evolution within the Galactic disc. As clusters pass through the disc, their orbits, shaped by gravitational interactions and the surrounding stellar populations, provide clues to their past trajectories and the environmental conditions that have influenced their evolution. At the same time, the metallicity of these clusters serves as a key indicator of their formation history, reflecting the chemical evolution of the disc and the enrichment processes that have taken place over cosmic timescales (Nilakshi et al., 2002; Ishchenko et al., 2025). This intricate relationship between orbital dynamics

and metallicity not only enhances our understanding of individual clusters, but also contributes to a more holistic understanding of Galactic structure, stellar population dynamics, and the broader implications for stellar evolution in different environments.

1.1. Previous Studies of King 2 and King 5

King 2 is among the oldest open clusters (OC) in the Milky Way, with an estimated age of 6 Gyr and a distance of 5700 pc (Table 1). It has not been extensively studied due to its substantial distance and lack of detailed membership data. The coordinates of King 2 are $(\alpha, \delta)_{2000} = (00^{\text{h}}51^{\text{m}}00^{\text{s}}, +58^{\text{d}}11^{\text{m}}00^{\text{s}})$ and $(l, b) = (122^{\circ}.874, -4^{\circ}.688)$. The first optical CMD for this distant cluster was presented by Kaluzny (1989b) using *BV* CCD photometry, giving a range of possible ages and distances based on various assumptions about reddening and metallicity. The distance of King 2 from the Galactic center was estimated to be about 14 kpc. A more comprehensive study was subsequently carried out by Aparicio et al. (1990, A90 hereafter) using *UBVR* photometric data. Assuming solar metallicity, they determined the age of the cluster to be 6 Gyr and the distance to be 5.7 kpc. They also reported significant binarity in the main sequence (MS) population.

Using spectroscopic data, Warren & Cole (2009, WC09 hereafter) determined a metallicity of $[\text{Fe}/\text{H}] = -0.42 \pm 0.09$ (dex). This iron abundance is poorer than the estimated solar abundance and contradicts the findings of A90. WC09 also finds a distance of 6.5 kpc and a slightly younger age of about 4 Gyr, with an CMD for the 2MASS K_s cluster reddening $E(B - V) = 0.31$ mag, which gives a better fit if a reddening value of 0.31 mag is adopted. This distance places King 2 at a Galactic radius of about 13 kpc, and its metallicity is in good agreement with the trends observed in the Galactic abundance gradients derived by Joshi, Deepak, & Malhotra (2024). Until the publication of *Gaia* DR2 (Gaia Collaboration et al., 2018), no proper motion studies had been performed for this cluster. However, Cantat-Gaudin et al. (2018) provided a membership catalogue for King 2, identifying 128 members using *Gaia* DR2 data. Subsequently, Jadhav et al. (2021) presented a kinematic membership analysis using *Gaia* DR3 kinematic data, identifying 1072 stars, of which 340 are classified as possible members. The optical photometric studies mentioned above indicate a significant presence of post-main-sequence hot stars in King 2.

Phelps et al. (1994) and Carraro & Vallenari (2000) studied King 5 photometrically and found it to be of Hyades age (~ 1 Gyr old). Carraro & Vallenari (2000) estimated the distance of King 5 located at $(\alpha, \delta)_{2000} = (03^{\text{h}} 14^{\text{m}} 45^{\text{s}}, 52^{\text{d}} 41^{\text{m}} 12^{\text{s}})$ and $(l, b) = (143^{\circ}.776, -4^{\circ}.287)$ as 1.90 kpc from the Sun. Durgapal et al. (1998) presented preliminary findings on this cluster.

The analysis of various kinematic parameters enhances our understanding of the dynamics of these OCs, establishing a framework for future investigations. Our findings underscore the relevance of these OCs in the context of stellar population studies, paving the way for further research into their formation and evolution. The classification of King 2 and King 5 within the young disk of the Milky Way reflects their relative youth

Table 1. The estimated values of color excess ($E(B - V)$), distance (d), metallicity ([Fe/H]) and age (t) for King 2 and King 5.

$E(B - V)$ (mag)	d (pc)	[Fe/H] (dex)	t (Gyr)	Ref
King 2				
0.23 to 0.50	7000	–	4 to 6	(1)
0.31 ± 0.02	5697 ± 65	-0.50 to -2.2	6.0	(2)
0.31	5750	-0.42 \pm 0.09	6.02	(3)
King 5				
–	–	–	1	(4)
–	1900	0.08	1	(5)

(1) Kaluzny (1989b), (2) Aparicio et al. (1990), (3) Dias et al. (2002), (4) Phelps et al. (1994), (5) Carraro & Vallenari (2000).

compared to older globular clusters, which exceed ten billion years in age. Despite being over a billion years old, these clusters reside in a dynamic region characterized by ongoing star formation and evolving stellar populations. Their inclusion in the young disk highlights the complex interplay of age, kinematics, and chemical characteristics that define stellar systems in this region. This perspective is supported by studies on the young disk's formation history and dynamics, emphasizing the importance of recognizing these older OCs as part of a more active stellar environment.

The article is divided into the following sections: Section 2 deals with a description of the astrometric and photometric data from the *Gaia* DR3 catalog. Section 3 is devoted to the structural properties and derivation of their fundamental parameters. In Section 4, we present our study of their photometric parameters (reddening, distance modulus, and ages) while the luminosity and mass functions are described in detail in Section 5. In Section 6, we discuss their dynamic evolution at different times. Section 7 presents velocity ellipsoid parameters, convergent point analysis, and their morphology in 3D. Our conclusions are given in Section 8.

2. Data and Analysis

2.1. The *Gaia* DR3 Data

We used fundamental parameters from prior studies on the open clusters King 2 and King 5 as initial values for this analysis. For the purpose of our analysis of the two clusters, we have downloaded the astrometric and photometric data with a radius of 30' from the *Gaia* Data Release (Gaia Collaboration et al., 2023)‡ hereafter DR3. Identification maps of King 2 and King 5 are shown in Figure 1. *Gaia* provides raw data collected by the European Space Agency's (ESA) *Gaia* mission§ during its continuous

‡ <https://cdsarc.cds.unistra.fr/viz-bin/cat/I/355>

§ <https://www.cosmos.esa.int/gaia>

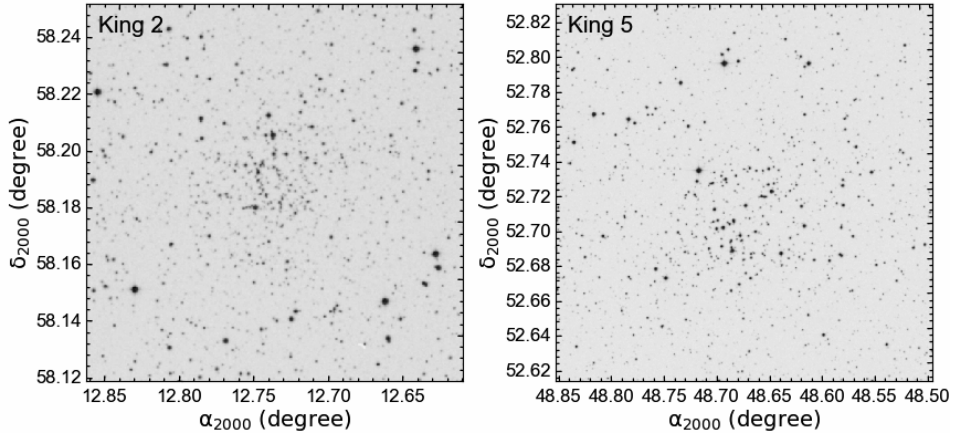


Figure 1. Identification maps of both OCs; King 2 (left) and King 5 (right).

sky scanning by the *Gaia* Data Processing and Analysis Consortium (DPAC)¶. *Gaia* DR3 represents a significant advance in the mission’s objectives for stellar, galactic and extragalactic studies. This release indicates that the evolution of the catalogue has become significantly more stable, exhibiting far fewer alterations between *Gaia* DR2 and DR3 than observed during the transition from *Gaia* DR1 to DR2. Notably, 97.5% of the catalogued sources have been maintained consistently across these two releases. The updated merging and split criteria reduce the number of superseded as well as new sources. *Gaia* DR3 has revolutionized the study and analysis of OC morphology by providing parallaxes with $\sim 30\%$ higher precision and proper motions with double accuracy, as compared to those in the *Gaia* DR2 (Gaia Collaboration et al., 2018).

Gaia DR3 provides five key quantities for nearly 1.8 billion stars and non-stellar objects (Gaia Collaboration et al., 2023), including their central coordinates (α , δ), proper motion components ($\mu_\alpha \cos \delta$, μ_δ), and trigonometric parallaxes (ϖ). The dataset covers sources with a limiting magnitude range from 3 to 21 in the G band and includes radial velocity measurements (V_r) for a limited number of entries. The precision of the *Gaia* DR3 astrometry is exceptional, with parallax errors ranging from 10 to 100 μ as and proper motion uncertainties generally being more precise between 20 and 140 μ as yr^{-1} though it is acknowledged that some proper motion errors may be negative. In addition to the astrometric data, *Gaia* photometry is provided in three bands: G , G_{BP} , and G_{RP} (Riello et al., 2021), covering the optical spectrum from 330 to 1050 nm, 330 to 680 nm, and 630 to 1050 nm, respectively. To enhance data quality, *Gaia* has improved its methods for estimating background noise in all three photometric bands. This ensures more accurate measurements of celestial objects by accounting for background light variations.

In *Gaia* DR3 the number of available observations per source is on average higher than in *Gaia* DR2. The parallax uncertainties for $G \leq 15$ mag sources are typically in the range of 0.02 - 0.03 mas, and about 0.07 mas for $G \sim 17$ mag sources. For the proper

¶ <https://www.cosmos.esa.int/web/gaia/dpac/consortium>

Table 2. Mean internal photometric errors for G and $(G_{\text{BP}} - G_{\text{RP}})$ magnitudes per G magnitude bin for the King 2 and King 5 OCs for sources within $30'$.

G	King 2			King 5		
	N	σ_G	$\sigma_{G_{\text{BP}} - G_{\text{RP}}}$	N	σ_G	$\sigma_{G_{\text{BP}} - G_{\text{RP}}}$
(06, 14]	183	0.0028	0.0028	171	0.0028	0.0024
(14, 15]	218	0.0028	0.0028	212	0.0028	0.0021
(15, 16]	462	0.0028	0.0028	429	0.0028	0.0021
(16, 17]	854	0.0028	0.0028	797	0.0029	0.0058
(17, 18]	1550	0.0029	0.0029	1416	0.0030	0.0152
(18, 19]	2402	0.0032	0.0032	2280	0.0033	0.0373
(19, 20]	3259	0.0040	0.0040	3549	0.0045	0.0818
(20, 21]	3309	0.0071	0.0071	3612	0.0083	0.1526

motion components, the uncertainties are as low as $0.01 - 0.02 \text{ mas yr}^{-1}$ for sources with $G < 15$ mag, increasing to approximately 0.4 mas yr^{-1} for sources with $G \sim 20$ mag. Table 2.1 shows the mean errors for G magnitudes and $(G_{\text{BP}} - G_{\text{RP}})$ color indices of stars in the King 2 and King 5 clusters as a function of G magnitudes. Figure 2, left and right panels, shows the photometric errors in G band, the color index $(G_{\text{BP}} - G_{\text{RP}})$, the trigonometric parallax and the proper motion components as a function of G magnitude for King 2 and King 5 for sources within $30'$, respectively, based on *Gaia* DR3 data.

2.2. Data Analysis

A new set of open-source tools has been developed for the study of structural parameters (e.g., radial density profiles, clusters radii, and membership probabilities), as well as cluster's fundamental parameters (reddening, distance modulus, age, and mass) either automatically or semi-automatically with the aid of the Automated Stellar Cluster Analysis package (AStECA; Perren et al. (2015))¶. A detailed description of the functions built within this tool can be found in Perren et al. (2015). The AStECA code is comprised of three principal independent analysis modules. The initial module is the structure study, which entails the identification of a cluster region based on an observed over-density of stars. The second module is concerned with the estimation of individual membership probabilities for stars situated within the over-density region. The final module is dedicated to the search for the best-fit parameters that describe the cluster's fundamental properties.

3. Structural Parameters

3.1. Determination of the Clusters' Centers

The central coordinates of King 2 and King 5 were estimated using the AStECA package, which adheres to the established methodology of assigning the clusters' center

¶ <https://asteca.readthedocs.io/en/latest/about.html>

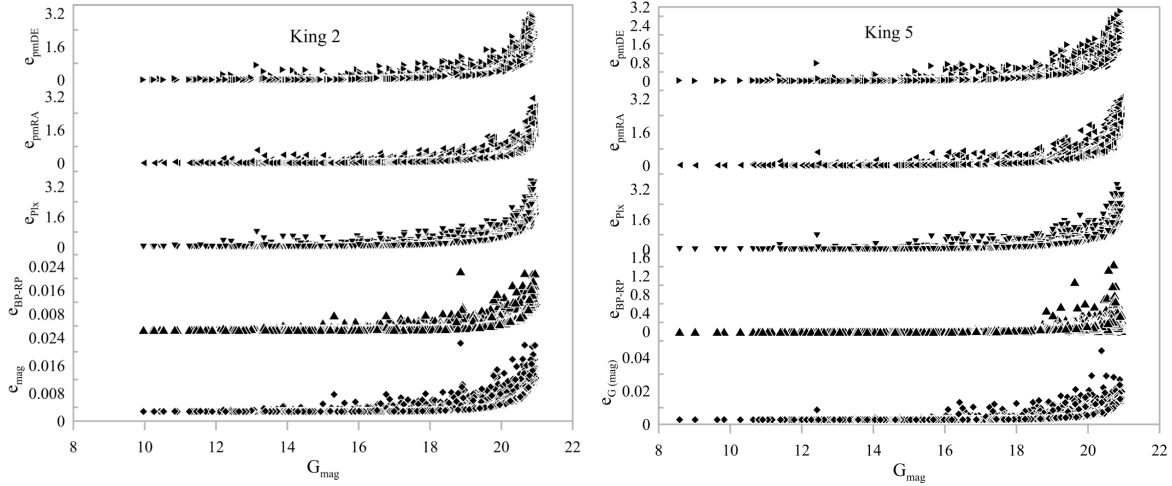


Figure 2. The *left panel* and *right panel* are the photometric errors in *Gaia* *G* errors, color index ($G_{\text{BP}} - G_{\text{RP}}$), parallax, and proper motions versus *G* magnitude passbands for King 2 and King 5 respectively.

to the location of maximum spatial density (Perren et al., 2015), ASTECA achieves this by fitting a two-dimensional Gaussian kernel density estimator (KDE) to the positional diagram of the cluster and identifying the peak value, as illustrated in Figure 3. In contrast to other algorithms that necessitate initial input values, ASTECA operates without them in fully automatic mode (although semi-automatic operation is feasible), thereby ensuring consistent convergence.

Furthermore, this method eliminates the necessity for region binning, as the kernel bandwidth is calculated using Scott's rule (Scott, 1992). By concurrently estimating the maximum density in both spatial dimensions, it circumvents potential inaccuracies in central coordinate determination, particularly in densely populated fields. Additionally, this approach is independent of the coordinate system, rendering it suitable for positional data stored in either pixel units or degrees. We redetermined the centers in right ascension and declination for King 2 and King 5 using ASTECA which is shown in Figure 3. The contours indicates cluster surface density (stars per arcmin^{-2}), where the blue and red colors refers to low and high densities regions for King 2 and King 5, respectively.

For King 2, equatorial coordinates (α, δ) were determined by this study as $(00^{\text{h}}50^{\text{m}}57^{\text{s}}.90, 58^{\circ}11'21''.20)$, compared to $(00^{\text{h}}50^{\text{m}}57^{\text{s}}.30, 58^{\circ}11'14''.49)$ in Hunt & Reffert (2023). Similarly, the Galactic coordinates of the OCs (l, b) were recalculated as $(123^{\circ}.26, -04^{\circ}.41)$, in this study, while Hunt & Reffert (2023) found it to be $(122^{\circ}.868, -04^{\circ}.686)$. For King 5, the equatorial coordinates (α, δ) were determined to be $(03^{\text{h}}14^{\text{m}}44^{\text{s}}.40, 52^{\circ}41'47''.83)$ in this study, compared to $(03^{\text{h}}14^{\text{m}}42^{\text{s}}.53, 52^{\circ}42'11''.28)$ in Hunt & Reffert (2023). The Galactic coordinates (l, b) were determined as $(144^{\circ}.14, -03^{\circ}.83)$ in this study and $(143^{\circ}.761, -04^{\circ}.276)$ in Hunt & Reffert (2023), slightly different from the earlier report. This comparison demonstrates that, while the recalculated center positions for both clusters show slight deviations from the values

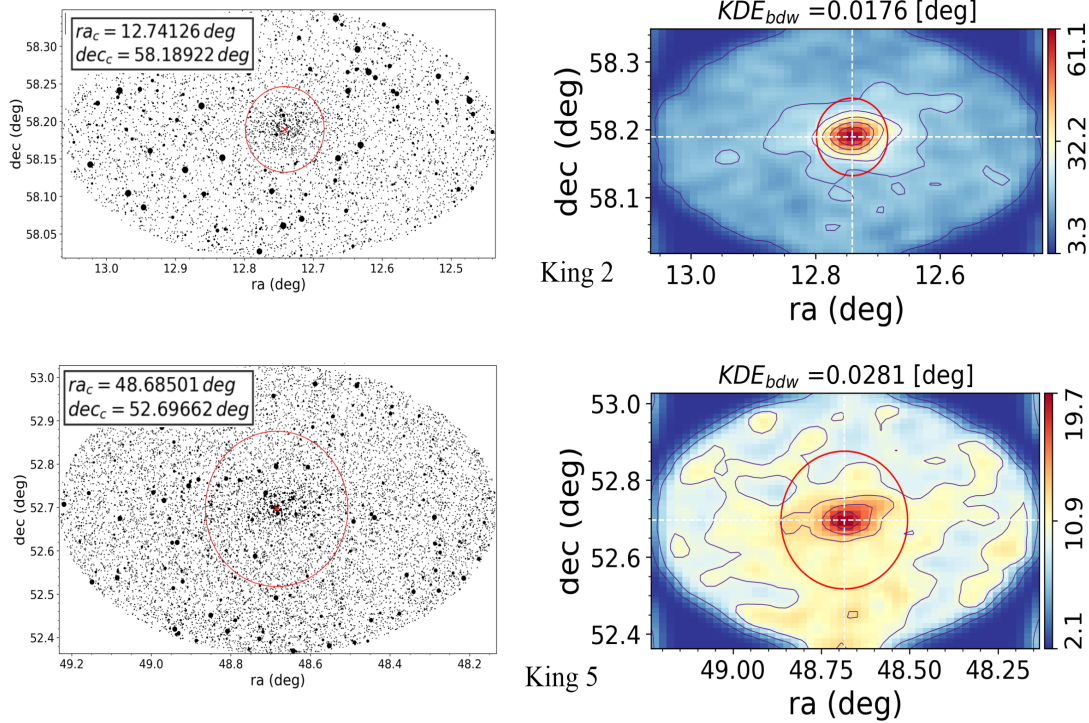


Figure 3. Left panel: the cluster's map charts defining the cluster regions with red circle centered by x-red symbol. Right panel: the contours of the cluster's surface density (stars per arcmin $^{-2}$) with color bars ranged from low (blue) to high (red) for both King 2 and King 5 OCs in the upper and lower panels, respectively.

reported by Hunt & Reffert (2023), these differences are within acceptable margins of uncertainty, suggesting that the new estimations refine rather than significantly alter the previously established coordinates, thereby enhancing the precision of the cluster's spatial parameters.

3.2. Radial Density Profiles and Radius of the Clusters

After we re-estimated the centers, the next step was to construct a radial density profile (RDP); every point of the RDP was obtained by generating rings (i^{th} zones) around the center defined for the potential cluster, i.e., the comparison field. The number density of stars (ρ_i) in the i^{th} zone is calculated as $\rho_i = N_i/A_i$, where N_i and A_i denote the number of stars and the area of the i^{th} zone, respectively. Creating a King profile (King, 1962) for this distribution, a smooth dashed line has been produced with the assistance of the ASTECA code (Perren et al., 2015). The method allowed us to estimate the internal cluster structural parameters as shown in Figure 4, where the values have large uncertainties, this might be due to the non-spherical geometry of these OC regions. The King's density ($\rho(r)$) profile (King, 1962), depends on core radius (r_c) (i.e., radial distance) at which the value of $\rho(r)$ becomes half of the central density (ρ_o) and on the background surface density (ρ_{bg}). In expansion, we will define the cluster radius (r_{cl}) at

Table 3. Structural properties of the King 2 and King 5 OCs obtained in this study.

Cluster	ρ_o (stars arcmin $^{-2}$)	ρ_{bg}	r_{cl} (arcmin) _{AStECA}	r_c (arcmin) _{AStECA}	r_t	r_c (pc)	r_t (pc)	δ_c	C
King 2	45.90 ± 0.67	8.15 ± 1.60	$6.94^{+0.22}_{-1.06}$	$1.44^{+0.20}_{-0.16}$	$14.04^{+2.28}_{-2.12}$	3.15 ± 0.56	30.83 ± 5.55	6.64 ± 0.44	4.83 ± 0.46
King 5	15.30 ± 0.39	5.75 ± 3.45	$11.33^{+5.45}_{-2.16}$	$2.78^{+0.53}_{-0.40}$	$22.61^{+3.08}_{-2.97}$	2.04 ± 0.70	16.59 ± 4.08	3.66 ± 0.68	4.08 ± 0.50

which the King profile intersects with background surface density ρ_{bg} . At this point the background star density ρ_b is given by ($\rho_b = \rho_{bg} + 3\sigma_{bg}$), where σ_{bg} is the uncertainty of ρ_{bg} (Bukowiecki et al., 2011).

In this study, we have calculated both the density contrast parameter (δ_c) and the concentration parameter (C) for these clusters for the first time. δ_c is defined as the stellar density contrast of the clusters in question relative to the background population (i.e., $\delta_c = 1 + \rho_o / \rho_{bg}$), therefore, its a measure of the compactness of the cluster (Bonatto & Bica, 2009) and C is defined by Peterson & King (1975) represents the ratio between r_{cl} and r_c , thereby providing insight into the cluster's structure. The computed values for both the density contrast parameter and the concentration parameter for King 2 and King 5 are presented in Table 3.

It is notable that δ_c assumes relatively high values, spanning the range $7 \lesssim \delta_c \lesssim 23$ (Bonatto & Bica, 2009). We calculated δ_c as 6.64 ± 0.44 and 3.66 ± 0.68 for the clusters King 2 and King 5, respectively. Since these two clusters are old ones, as the ages of OC's increase, stellar dynamics within the clusters influence the central part of the cluster to become circular (Fujii & Portegies Zwart, 2016; Qin et al., 2024; Pera et al., 2024).

By combining both the r_{cl} and r_c to characterise clusters and their structures, Peterson & King (1975) provided a framework for interpreting cluster sizes. Nilakshi et al. (2002) found that the angular size of the coronal region typically extends to about $6r_c$, while Bukowiecki et al. (2011) showed that r_{cl} can range from $2r_c$ to $7r_c$. In our analysis, as shown in Table 3, C for King 2 and King 5 are approximately 4.83 ± 0.46 and 4.08 ± 0.50 , respectively, which agrees well with the results of Bukowiecki et al. (2011). In addition, Hunt & Reffert (2023) reported the r_c for King 2 and King 5 to be 2.375 and 1.728 pc respectively, with r_t of 19.911 and 7.906 arcminutes, indicating that both clusters exhibit a well-defined structure and size that aligns with their dynamical status and evolutionary history as observed in previous studies.

4. Photometric Analysis: Reddening, Distance and Age

4.1. Decontamination of the Cluster from Field Stars

To determine the fundamental astrophysical properties of the clusters, including reddening, distance modulus, and age, a photometric analysis was conducted through the construction of a color-magnitude diagram (CMD). Identifying probable members is crucial in reducing contamination from field stars. Various decontamination techniques have been developed and extensively discussed in the literature to statistically eliminate field stars. Among these methods, proper motions (PMs) provide a robust approach for

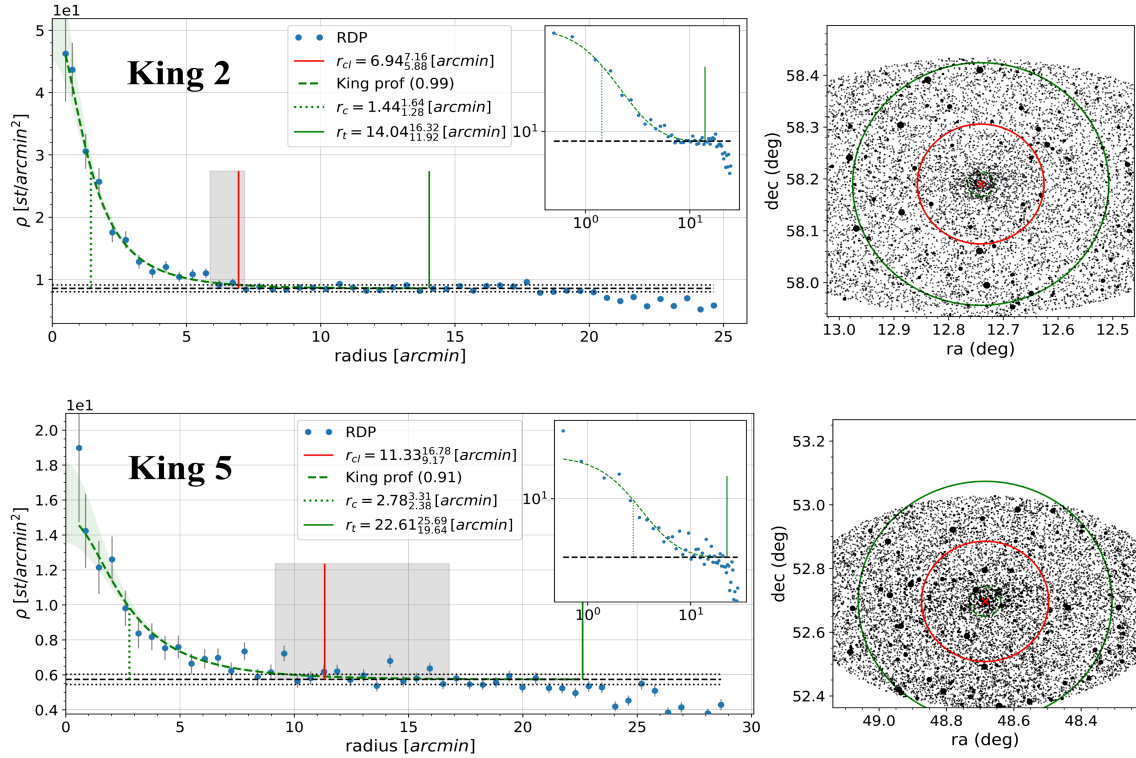


Figure 4. The RDP for King 2 and King 5 OCs were generated using the ASTECA code, with the results shown as blue dots. The green dashed line and shaded region represent King's density profile. Additionally, the black dashed line indicates the background field density (ρ_{bg}), while the dotted black line marks the central surface density (ρ_0). Vertical lines are used to denote the structural parameters, including the core radius (r_c), the limiting radius (r_{cl}), and the tidal radius (r_t).

estimating membership probabilities with higher accuracy. In this study, membership probabilities were assigned based on the rigorous selection criteria implemented in the second module of the ASTECA code, following the methodology described by Cabrera-Cano & Alfaro (1990); El Aziz, Selim, & Essam (2016).

The study by Perren et al. (2015) utilized the ASTECA code to estimate the number of probable cluster members through two different approaches. The first approach computes the radial density profile (RDP) within the tidal radius (r_t), relative to the density of background stars, utilizing a King model with three parameters (3P). The effectiveness of this approach depends on obtaining a well-constrained r_t and achieving convergence in the 3P fitting process; otherwise, the estimated member count may be significantly overestimated. The second method relies on direct star counts, where the expected number of field stars (n_{fl}) within the cluster area is calculated as the product of the background density (d_{field}) and the cluster area (A_{cl}), determined from the cluster radius (r_{cl}). Subtracting this field star estimate from the observed total star count within r_{cl} ($n_{\text{cl+fl}}$) yields the final estimated cluster membership (n_{cl}).

Both methods depend on completeness limits, as they estimate the number of member stars down to the faintest observed magnitudes. Using the ASTECA code,

the most probable members of King 2 and King 5 clusters were determined as 340 and 403, respectively, with a membership probability threshold of $P_{\text{AStECA}} \geq 50\%$.

To derive the mean proper motion components of the clusters, Gaussian fitting was applied to the distributions of probable members in each coordinate direction, as shown in Figure 5 (upper panel). To ensure the reliability of these results, the analysis was restricted to stars with positive parallax values, as depicted in Figure 5. The mean proper motion components in right ascension and declination were calculated for both clusters and are presented in Table 3. Additionally, the trigonometric parallaxes of the member candidates were used to construct histograms for King 2 and King 5, from which the mean parallax values were obtained. These results indicate distances of $d_{\varpi} = 5556 \pm 1512$ pc for King 2 and $d_{\varpi} = 2439 \pm 190$ pc for King 5.

The AStECA code was further employed to estimate astrophysical parameters such as reddening, distance modulus, and age using photometric data in the G , G_{BP} , and G_{RP} passbands. The code utilizes the PARSEC v1.2S⁺ theoretical isochrones (Bressan et al., 2012) and the Kroupa (2002) initial mass function (IMF). As illustrated in Figure 6, the CMDs in G vs. $(G_{\text{BP}} - G_{\text{RP}})$ were fitted with a dense grid of isochrones with metallicities $z = 0.0088$ and $z = 0.0109$, yielding ages of $t = 4.8 \pm 0.3$ Gyr for King 2 and $t = 1.45 \pm 0.1$ Gyr for King 5.

To convert the metallicity parameter z into [Fe/H], the transformation provided by Bovy* was used, which is consistent with PARSEC isochrone models (Yontan et al., 2022; Çakmak et al., 2024):

$$z_x = \frac{z}{0.7515 - 2.78 \times z} \quad (1)$$

and

$$[\text{Fe}/\text{H}] = \log(z_x) - \log\left(\frac{z_{\odot}}{1 - 0.248 - 2.78 \times z_{\odot}}\right) \quad (2)$$

where z_x is an intermediate variable, and the solar metallicity is assumed to be $z_{\odot} = 0.0152$ (Bressan et al., 2012). Applying these equations, the metallicity values for King 2 and King 5 were determined as $z = 0.0088$ ([Fe/H] = -0.25 dex) and $z = 0.0109$ ([Fe/H] = -0.15 dex), respectively.

To correct for the effects of interstellar extinction, the reddening values were adjusted using the relation $E(G_{\text{BP}} - G_{\text{RP}}) = 1.289 \times E(B - V)$ (Casagrande & Vandenberg, 2018; Zhong et al., 2019), while the extinction coefficient in the G band was computed as $A_G = 2.74 \times E(B - V)$. The estimated reddening values were verified using the Stilism 3D dust maps‡ (Capitanio et al., 2017). The distance modulus derived from CMD fitting for King 2 and King 5 clusters was found to be $(m - M)_0 = 14.896 \pm 0.053$ and 13.321 ± 0.038 mag, respectively. These correspond to photometric distances of $d_{\text{phot}} = 6586 \pm 164$ pc for King 2 and $d_{\text{phot}} = 2220 \pm 40$ pc for King 5. A summary of the obtained astrophysical and photometric parameters is provided in Table 4.

⁺ <http://stev.oapd.inaf.it/cgi-bin/cmd>

* <https://github.com/jobovy/isodist/blob/master/isodist/Isochrone.py>

‡ <https://stilism.obspm.fr>

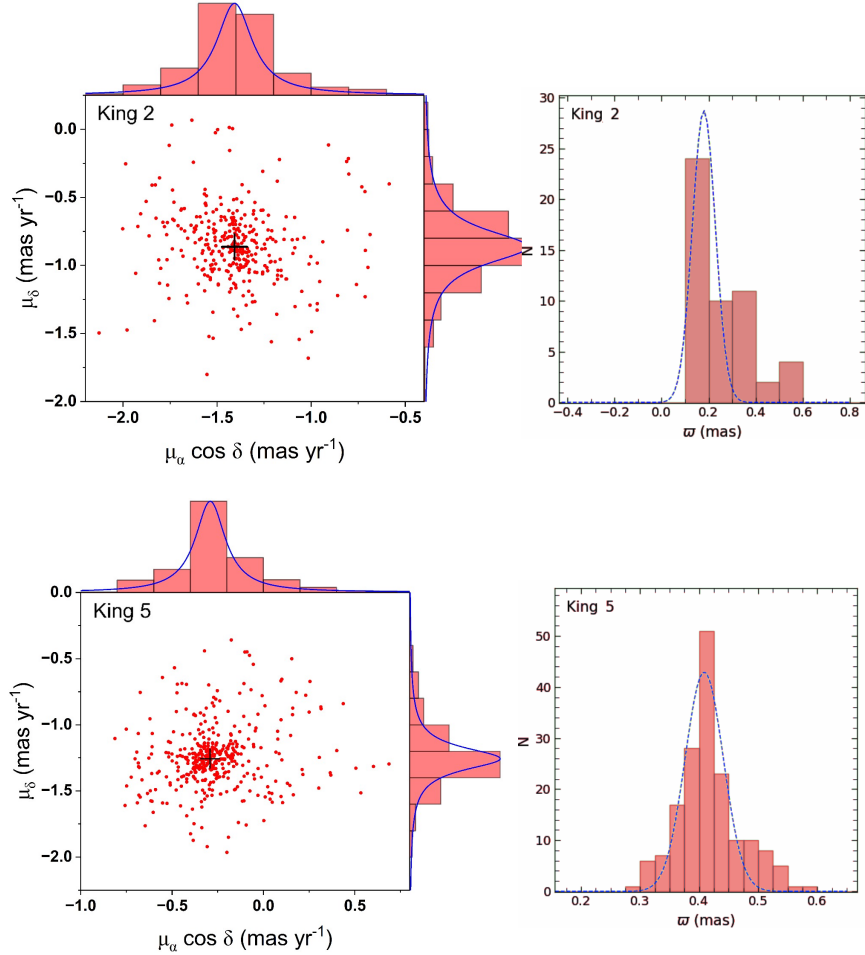


Figure 5. *Upper panel:* The distribution of the mean PM ($\mu_\alpha \cos \delta$, μ_δ). *Lower panel:* Normalised trigonometric parallax (ϖ) distribution for the entirety of the stellar member candidates within the cluster space

Using our estimated distances d , we infer the clusters' distances to the Galactic center R_{gc} (i.e., $R_{\text{gc}} = \sqrt{R_{\text{o}}^2 + (d \cos b)^2 - 2R_{\text{o}}d \cos b \cos l}$), where $R_{\text{o}} = 8.2 \pm 0.1$ kpc (Bland-Hawthorn et al., 2019), l is the Galactic longitude, and b is the Galactic latitude. The projected distances toward the Galactic plane (X_{\odot} , Y_{\odot}) and the distance from the Galactic plane (Z_{\odot}) takes the forms, $X_{\odot} = d \cos b \cos l$, $Y_{\odot} = d \cos b \sin l$, and $Z_{\odot} = d \sin b$. Results of these calculations for King 2 and King 5 are provided in Table 4.

4.2. Blue Straggler Stars

The identification of blue straggler stars (BSSs) lying above the MS turnoff region in CMDs depends on detailed analysis of photometric data, in particular precise measurements from *Gaia* DR3, which provides valuable insights into the membership probabilities and cluster characteristics (Leiner & Geller, 2021; Jadhav et al., 2021; Chand et al., 2024). BSS formation mechanisms, supported by models from Antonini

et al. (2016) and Sindhu et al. (2019), suggest that dense cluster environments provide ideal conditions for the formation of these massive stars, either through close stellar encounters or within primordial binaries. Gosnell et al. (2015) have shown that in older OCs, a significant fraction of BSS populations are likely to evolve from binary stars interactions - a formation pathway that may also be relevant for King 2 and King 5, given their ages.

Rain, Ahumada, and Carraro (2021) presented 22 and 4 BSS candidates, respectively, for King 2 and King 5. In this study, we identify potential 17 (King 2) and 4 (King 5) BSSs. These candidate BSSs, marked with a blue circle, are highlighted in Figure 6. Although the BSS identified in this study are based on previous classifications, further investigation into the connection between BSS and other stellar populations, such as the merging probability in clusters with different stellar densities, is needed.

5. Luminosity and Mass Functions

After we determined new structural and astrophysical parameters for the King 2 and King 5 open clusters, we used the *Gaia* DR3 data and analyzed it with the ASTECA packages. We estimate the luminosity functions, (LF) and mass functions (MFs), where the LF is defined as the distribution of members according to different absolute magnitudes; The upper panel of Figure 7 shows the LF member stars, and the corresponding total absolute luminosities M_G are listed in Table 5. OCs contain both low and high-mass stars which have the same morphology and formation within the same molecular cloud, this makes them the ideal objects to study the initial mass function IMF (Piatti et al., 2002; Yontan, 2023; Elsanhoury et al., 2024, 2025) which is defined as the number density dN of stars scattered over a logarithmic mass scale within a mass range dM , centered at mass M .

Both LF and MF are associated with each other by the well-known Mass-Luminosity Relation (MLR), then by accounting for absolute magnitudes M_G (mag) and the masses (M/M_\odot) combined with adopted isochrones (Bressan et al., 2012) on CMDs for estimated ages, distance modulus, and reddening, it is possible to infer the mass-luminosity ratio (MLR) of individual member stars with the second-order polynomial function with coefficients a_0 , a_1 , and a_2 with their uncertainty as well as the total mass $M_C(M_\odot)$ as presented in table 5. The present-day mass function (PDMF) and its dimensionless parameters or slope denoted by (α) is given by Salpeter (1955) as -2.35 and indicating the characteristics of massive stars ($> 1M_\odot$). Salpeter's power law suggests that the star count in each mass range decreases significantly as the mass increases. The values we obtained, $\alpha_{\text{King2}} = -2.62 \pm 0.02$ and $\alpha_{\text{King5}} = -2.08 \pm 0.01$, are consistent with the findings of Salpeter (1955).

The membership probability of a star is calculated based on the statistical assignment, where a star with a membership probability of 50% is considered to contribute fully to the luminosity function. This approach accurately represents the likelihood of inclusion in our analysis. The mass of stars in our study is derived using

Table 4. The astrometric and astrophysical parameters for King 2 and King 5, as obtained in this study herewith together with comparisons to other published values.

Parameter	King 2	King 5	Reference
N	340	403	This study
	458	454	Hunt & Reffert (2023)
$\langle \mu_\alpha \cos \delta \rangle$ (mas yr $^{-1}$)	-1.407 ± 0.008	-0.291 ± 0.005	This study
	-1.420 ± 0.006	-0.304 ± 0.005	Hunt & Reffert (2023)
	-1.358 ± 0.010	-0.282 ± 0.009	Cantat-Gaudin et al. (2018)
$\langle \mu_\delta \rangle$ (mas yr $^{-1}$)	-0.863 ± 0.012	-1.256 ± 0.005	This study
	-0.844 ± 0.007	-1.265 ± 0.005	Hunt & Reffert (2023)
	-0.824 ± 0.013	-1.200 ± 0.009	Cantat-Gaudin et al. (2018)
$\langle \varpi \rangle$ (mas)	0.180 ± 0.049	0.409 ± 0.032	This study
	0.162 ± 0.005	0.406 ± 0.003	Hunt & Reffert (2023)
	0.166 ± 0.010	0.367 ± 0.004	Cantat-Gaudin et al. (2018)
d_ϖ (pc)	5556 ± 1512	2439 ± 190	This study
	6173	2463	Hunt & Reffert (2023)
	6024	2725	Cantat-Gaudin et al. (2018)
$(m - M)_0$ (mag)	14.896 ± 0.053	13.321 ± 0.038	This study
	13.687	11.994	Hunt & Reffert (2023)
d_{Photo} (pc)	6586 ± 164	2220 ± 40	This study
	5240.828	2286.376	Hunt & Reffert (2023)
	5377.6	2549.9	Cantat-Gaudin et al. (2018)
z	0.0088	0.0109	This study
t (Gyr)	4.8 ± 0.3	1.45 ± 0.1	This study
$E(B - V)$ (mag)	0.306 ± 0.019	0.605 ± 0.013	This study
	0.5549	0.9999	Hunt & Reffert (2023)
$E(G_{\text{BP}} - G_{\text{RP}})$ (mag)	0.431 ± 0.027	0.853 ± 0.019	This study
X_\odot (kpc)	-3.006	-1.962	This study
	-2.778	-2.03	Cantat-Gaudin et al. (2018)
Y_\odot (kpc)	4.651	1.437	This study
	4.299	1.487	Cantat-Gaudin et al. (2018)
Z_\odot (kpc)	-0.454	-0.187	This study
	-0.419	-0.188	Cantat-Gaudin et al. (2018)
R_{gc} (kpc)	12.08	10.22	This study
	11.92	10.476	Cantat-Gaudin et al. (2018)

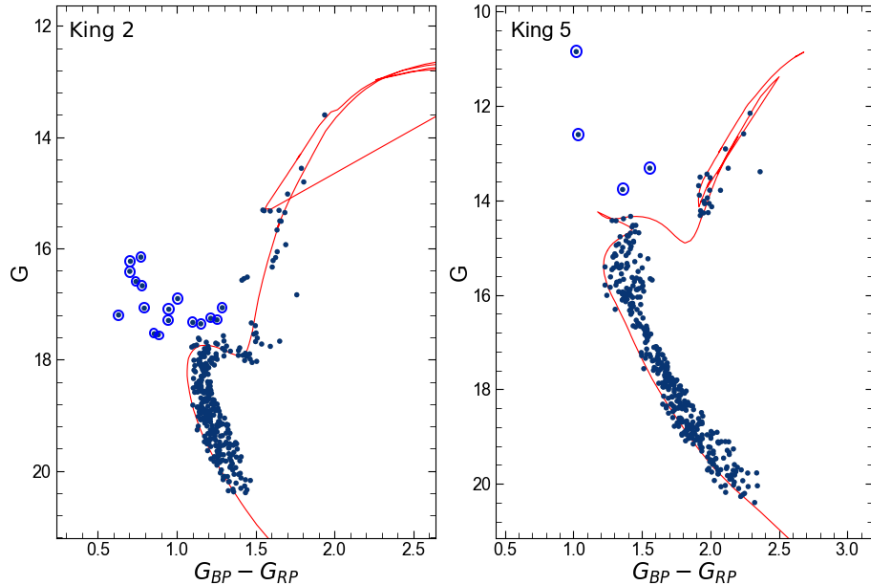


Figure 6. CMDs of King 2 and King 5 OCs. The fitted G versus $(G_{BP} - G_{RP})$ isochrones corrected by Bressan et al. (2012) are shown with red lines for different metallicities $Z = 0.0088$ (King 2) and 0.0109 (King 5) and t (Gyr) = 4.80 ± 0.30 (King 2) and 1.45 ± 0.10 (King 5). Blue circle represent BSS candidates.

Table 5. Obtained LFs and MFs results of King 2 and King 5 OCs with their α 's.

Parameter	King 2	King 5
$\langle M_G \rangle$ (mag)	3.686 ± 1.132	4.076 ± 1.820
a_0	1.18395 ± 0.0071	1.71670 ± 0.0051
a_1	0.04502 ± 0.0022	-0.03456 ± 0.0010
a_2	-0.0204 ± 0.0001	-0.01884 ± 0.0002
M_C (M_\odot)	356 ± 19	484 ± 22
$\langle M_C \rangle$ (M_\odot)	1.047	1.200
α	-2.62 ± 0.02	-2.08 ± 0.01

both the MLR and theoretical isochrones, ensuring reliable mass estimates across the observed population. Additionally, we factored out the contamination of field stars by employing the ASTECA code, which calculates membership probabilities based on proper motions and color-magnitude data.

The optimal fitting of the data to a straight line was performed using the least-squares method, and the resulting plots for the MF are presented in Figure 7 (lower panel). In this analysis, the M_G ranges for MFs calculations contain the stars with; $-1.293 \leq M_G$ (mag) ≤ 5.496 & $0.815 \leq M_C$ (M_\odot) ≤ 1.209 (King 2) and $-2.470 \leq M_G$ (mag) ≤ 7.367 & $0.440 \leq M_C$ (M_\odot) ≤ 1.732 (King 5).

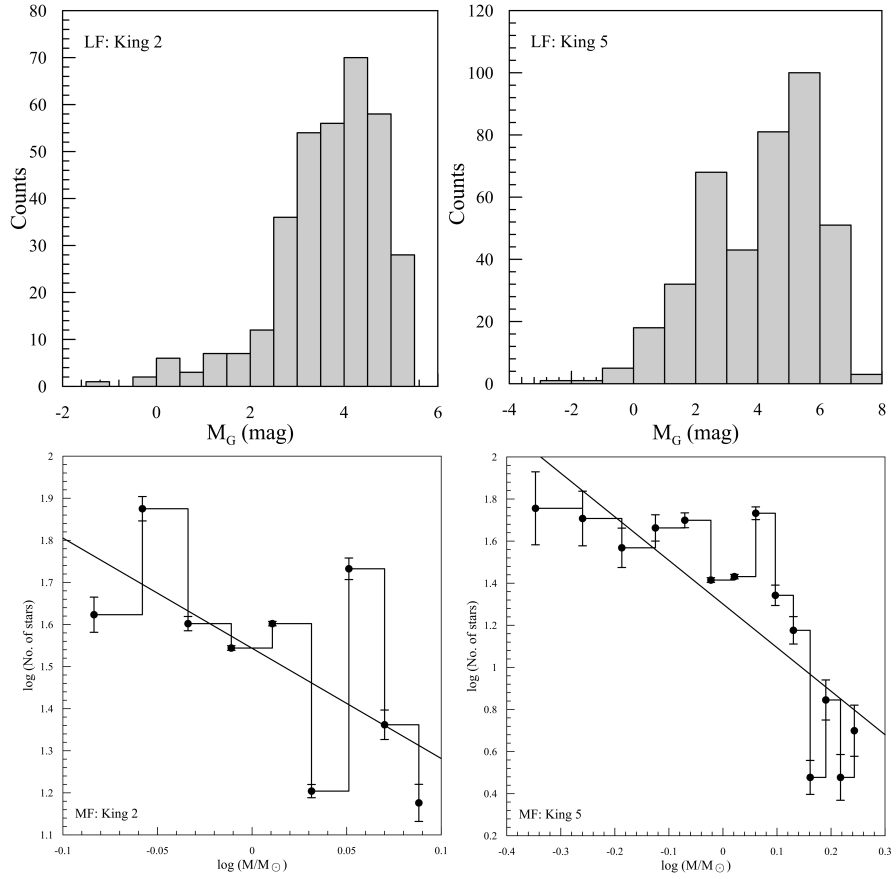


Figure 7. The true LF of King 2 (upper left panel) and King 5 (lower right panel), along with the MF of King 2 (lower left panel) and King 5 (lower right panel), are fitted using the power law from Salpeter (1955) to calculate the slope α .

6. Dynamical Evolution Times

Dynamically, OCs differ from their compact halo counterparts, such as globular clusters, due to the interactions among their stars leading to exchange energy (Baumgardt et al., 2022; Arnold & Baumgardt, 2025). OCs typically exhibit a looser spatial distribution than globular clusters. Processes such as mass segregation, whereby more massive stars concentrate towards the cluster core compared to fainter ones, have been observed in numerous OCs (Piatti, 2016; Zeidler et al., 2017; Dib & Basu, 2018; Rangwal et al., 2019; Bisht et al., 2020; Joshi et al., 2020). It has been demonstrated that, as the cluster evolves, its kinetic energy, represented by the velocity distribution of its stars, tends towards a Maxwellian equilibrium (Bisht et al., 2019). The characteristic time required for this dynamical evolution is known as the dynamical relaxation time, denoted by T_{relax} (yr). The mathematical form of this function was established by Spitzer & Hart (1971), and it depends on both the number N of member stars and the cluster diameter

Table 6. Dynamical evolution times and escape velocity for King 2 and King 5.

Cluster	T_{relax} (Myr)	τ_{ev} (Myr)	τ	V_{esc} (km s $^{-1}$)
King 2	59	5900	81.54	71.29 ± 8.44
King 5	35	3500	42.33	178.15 ± 13.35

($D \approx 2r_{\text{lim}}$). This function was further explored by Lada & Lada (2003):

$$T_{\text{relax}} = \frac{8.9 \times 10^5 N^{1/2} R_{\text{h}}^{3/2}}{\sqrt{\langle M_{\text{C}} \rangle} \log(0.4 N)} \quad (3)$$

The half-mass radius (R_{h}) values we obtained are 5.22 ± 0.44 pc and 3.10 ± 0.57 pc for the respective clusters. The mean mass of the members, $\langle M_{\text{C}} \rangle$, in solar masses can be determined using the transformation provided by (Sableviciute et al., 2006):

$$R_{\text{h}} = 0.547 \times r_{\text{c}} \times \left(\frac{r_{\text{t}}}{r_{\text{c}}}\right)^{0.486} \quad (4)$$

where r_{c} is the core radius and r_{t} is the tidal radius is defined as the distance at which a balance between two gravitational forces acts, one towards the Galactic center and another towards the cluster center, to keep the cluster is bound (Röser, 2019). The subsequent objective is to estimate the evaporation time ($\tau_{\text{ev}} \approx 10^2 T_{\text{relax}}$), which characterizes the time required for the ejection of all member stars due to internal stellar interactions (Alvarez Baena et al., 2024). Low-mass stars typically escape the cluster over time, primarily at low velocities through the Lagrange points (Kupper et al., 2015). To maintain the gravitational binding of the cluster, the escape velocity (V_{esc}), which is necessary for the rapid expulsion of gas, is computed using the relation ($V_{\text{esc}} = R_{\text{gc}} \sqrt{\frac{2GM_{\text{C}}}{3r_{\text{t}}^3}}$), as described by (Kafle et al., 2018; Hunt & Vasiliev, 2025), where R_{gc} represents the distance to the Galactic center, G is the gravitational constant, and M_{C} denotes the total mass of the cluster.

In conclusion, the dynamical state of King 2 and King 5 clusters can be described and defined, allowing the dynamical evolution parameter ($\tau = \text{age}/T_{\text{relax}}$) to be calculated. This demonstrates that the two clusters are dynamically relaxed. All our numerical results for these different dynamical evolution times are listed in Table 6.

7. VEPs and CP

In order to emphasise the gravitationally bound nature of the stellar groups within a confined volume of space within the Galactic system, we conducted a study of the velocity ellipsoid parameters (VEPs) and kinematics. This was achieved through the utilisation of a computational algorithm applied by Elsanhoury et al. (2022) using member stars with coordinates (α, δ) located at distances (d_i ; pc) and PMs ($\mu_{\alpha} \cos \delta, \mu_{\delta}$; mas yr $^{-1}$). To estimate the mean radial velocities of King 2 and King 5, we analyzed the

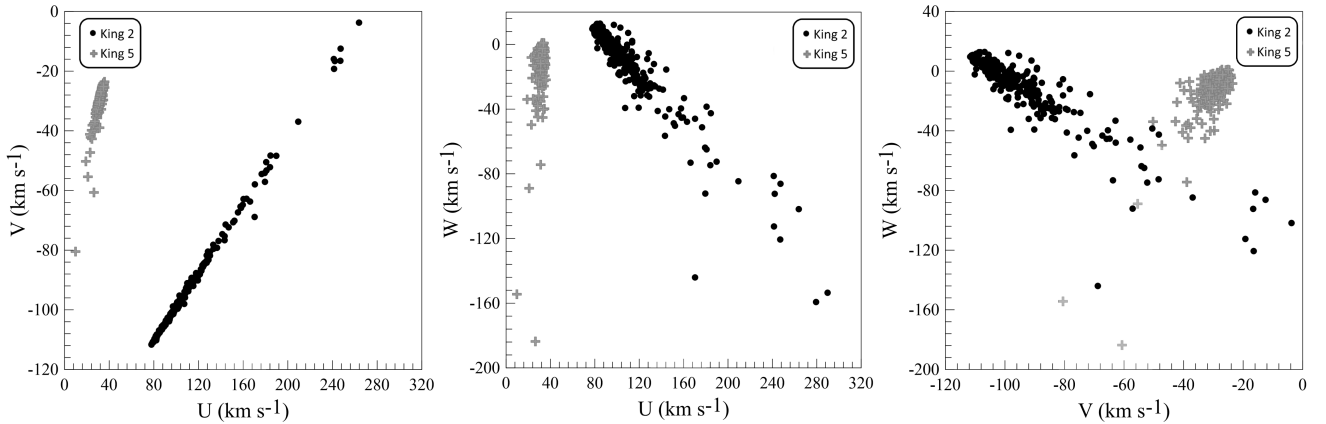


Figure 8. The distribution of the spatial space components (U , V , W) of the members of King 2 and King 5.

most probable members ($P \geq 50\%$ based on *Gaia* DR3 data. Following the methodology outlined by Soubiran et al. (2018), we applied their equations to derive mean radial velocity values for these clusters. (V_r ; km s^{-1}) are -136.34 ± 0.14 (King 2) and -41.94 ± 0.32 (King 5). In this context, the velocity components (V_x , V_y , V_z ; km s^{-1}) along the x , y , and z axes in a Sun-centered coordinate system, as well as the spatial space velocity components (U , V , W ; km s^{-1}) of the member stars on the celestial sphere, along with their Galactic coordinates, can also be calculated (see also, Haroon et al., 2024; Elsanhoury et al., 2022; Elsanhoury, 2021). These values are presented in Table 7. The distribution of these space velocities is shown in Figure 8. Based on the aforementioned analysis, we can determine the apex position, which represents a point in space, (A_o , D_o), toward which the member stars are collectively moving. This apex, known as the convergent point (CP), is identified by the intersection of the spatial velocity vectors of individual stars with the celestial sphere. We adopted the AD-diagrams method given by (Chupina et al., 2001), where they use the notion of an individual stellar apex in equatorial coordinates for the members through space velocity vectors (V_x , V_y , V_z). Therefore, $A_o = \tan^{-1}(\bar{V}_y/\bar{V}_x)$ and $D_o = \tan^{-1}(\bar{V}_z/\sqrt{\bar{V}_x + \bar{V}_y})$. Figure 9 gives the apex equatorial coordinates (A_o , D_o) for King 2 and King 5 OCs, and the numerical results devoted with Table 7.

7.1. Other Kinematic Structure Parameters

(a) The Cluster Center (x_c , y_c , z_c)

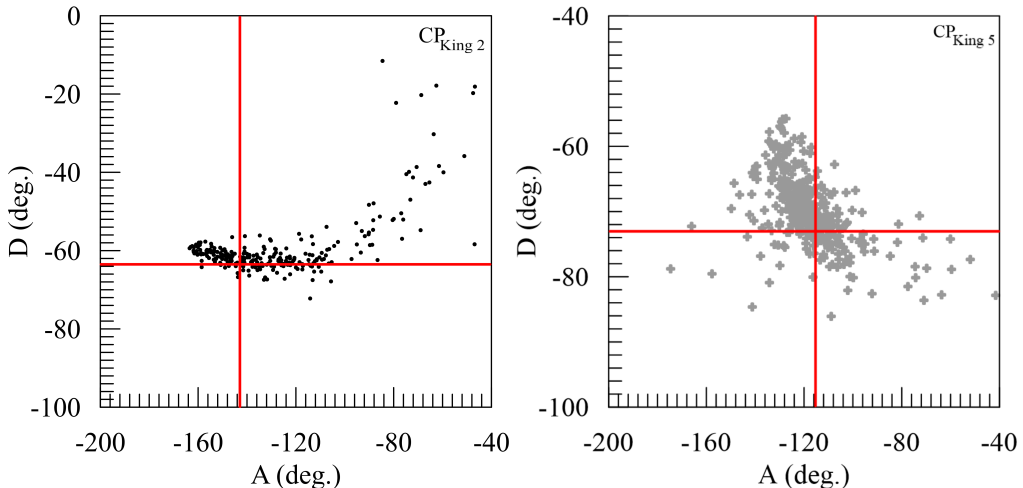
For N_i member stars located at a distance $d_i(\text{pc})$ with corresponding (α_i, δ_i) , the cluster center is x_c , y_c , and z_c (Elsanhoury et al., 2022) in units of pc and the obtained results are listed in table 7.

(b) The Solar Elements

The components of the Sun's velocities ($U_\odot = -\bar{U}$, $V_\odot = -\bar{V}$, and $W_\odot = -\bar{W}$) are S_\odot

Table 7. Dynamical evolution and kinematic parameters of King 2 and King 5 OCs.

Parameter	King 2	King 5
\bar{V}_X (km s $^{-1}$)	14.61 ± 3.82	-5.54 ± 2.35
\bar{V}_Y (km s $^{-1}$)	-112.58 ± 10.61	-11.83 ± 3.44
\bar{V}_Z (km s $^{-1}$)	-228.52 ± 15.12	-43.17 ± 6.57
A_o (°)	-142.61 ± 0.08	-115.10 ± 0.09
D_o (°)	-63.58 ± 0.14	-73.16 ± 0.12
\bar{U} (km s $^{-1}$)	172.27 ± 13.13	31.61 ± 5.62
\bar{V} (km s $^{-1}$)	-58.13 ± 7.60	-29.82 ± 5.46
\bar{W} (km s $^{-1}$)	-59.23 ± 7.70	-12.09 ± 3.48
x_c (kpc)	8.664 ± 0.09	1.118 ± 0.03
y_c (kpc)	1.961 ± 0.04	1.272 ± 0.04
z_c (kpc)	14.320 ± 0.12	2.224 ± 0.05
S_\odot (km s $^{-1}$)	191.22 ± 13.83	45.10 ± 6.72
(l_A, b_A) (°)	(18.65, 18.05)	(43.34, 15.55)
(α_A, δ_A) (°)	(-82.61, 53.58)	(64.91, 73.16)

**Figure 9.** Plots of the AD-diagrams for King 2 and King 5. The crosshair refers to the apex position (A_o , D_o) of the members.

$= \sqrt{(\bar{U})^2 + (\bar{V})^2 + (\bar{W})^2}$, and the position of the solar apex in Galactic coordinates is (l_A, b_A) and within equatorial coordinates is (α_A, δ_A) and are drawn like seen in Table 7.

(c) King's Morphology with 3D

We analyze the 3D spatial position of member stars in King 2 and King 5 OCs in heliocentric Cartesian coordinates X , Y , and Z (Elsanhouri et al., 2022). The 3D morphology for these OCs was plotted here in Figure 10; it is noticeable that the stars are located and expand through separate elongated regions in space. This phenomenon may be regarded as a rapid expulsion and virilization of gas (Pang et al., 2021) and

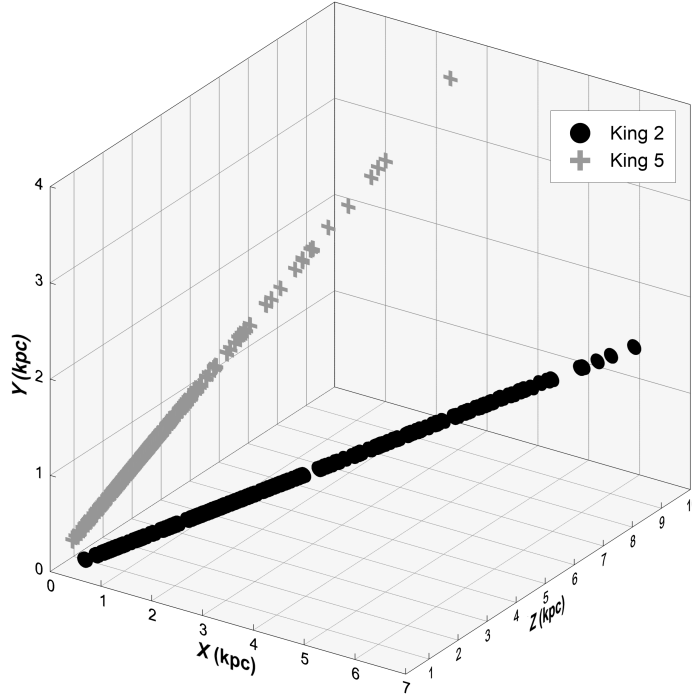


Figure 10. The two clusters, designated King 2 and King 5, are illustrated using 3D spatial morphology plots in heliocentric cartesian coordinates (X , Y , Z ; kpc).

Table 8. Dynamic orbit parameters of King 2 and King 5 OCs.

Cluster	Z_{\max} (kpc)	R_a (kpc)	R_p (kpc)	R_m (kpc)	e	T_p (Myr)
King 2	0.499 ± 0.246	13.076 ± 1.555	7.379 ± 2.024	10.227 ± 1.789	0.279 ± 0.072	297 ± 6
King 5	0.177 ± 0.023	10.302 ± 0.115	9.132 ± 0.232	9.717 ± 0.174	0.060 ± 0.008	277 ± 5

accordingly, it can be inferred that the birthplaces of stars are likely located within the same area of the Galactic disc. This suggests that these OCs may have formed from a similar environment or molecular cloud, highlighting their potential shared origins.

(d) Dynamic Orbit Parameters

The methodology used in this study, which has been successfully applied to both individual stars and other star clusters, allows for a comprehensive analysis of the distribution and dynamics of OCs in the Milky Way (Yontan & Canbay , 2022; Taşdemir & Yontan, 2023; Yucel et al., 2024). This approach is important for understanding the structure and evolutionary processes of our Galaxy. We determined the Galactic populations of King 2 and King 5 by analyzing the kinematics and dynamics of the clusters' orbits (Dursun et al., 2024; Taşdemir & Çınar, 2025). We also carried out a detailed kinematic analysis, including the calculation of the space velocity components, Galactic orbital parameters and formation radii of the clusters (see Section 7).

In conducting orbital analyses, we employed the MWpotential2014 model,

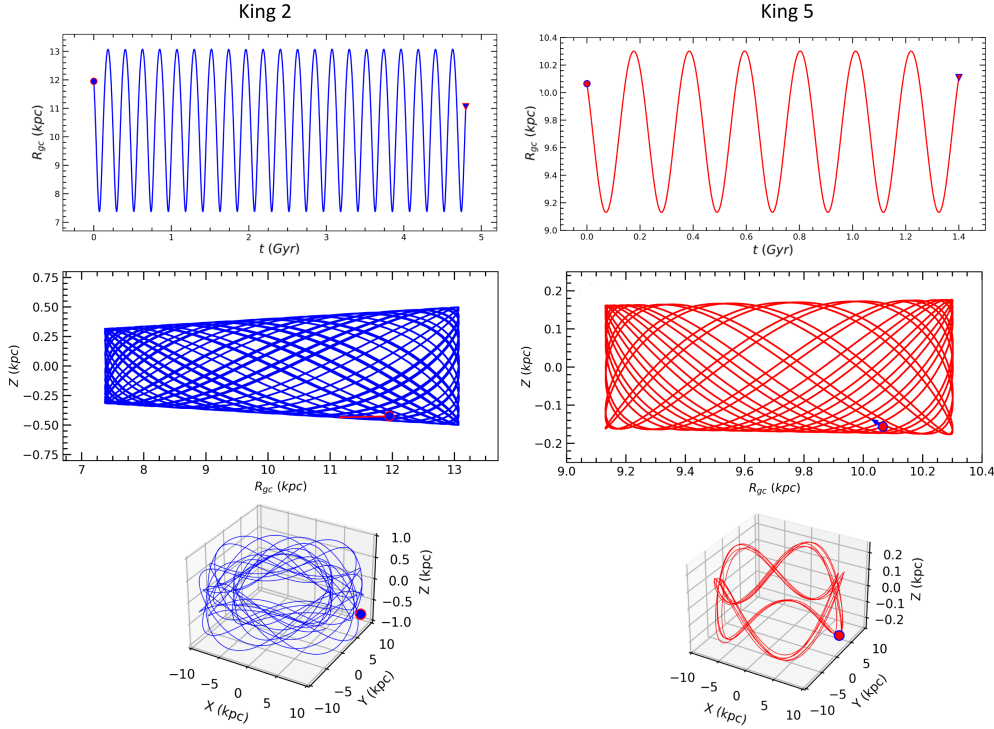


Figure 11. The Galactic orbits and birth radii of King 2 and King 5 are illustrated on three different planes: $R_{\text{gc}} \times t$ (top), $Z \times R_{\text{gc}}$ (middle), and $X \times Y \times Z$ (bottom).

which is integrated within the GALPY^{††} package. This package is a library that facilitates the study of galactic dynamics and was developed by Bovy (2015). This model incorporates several key parameters, including the Galactocentric distance ($R_{\text{gc}} = 8.20 \pm 0.10$ kpc) and the orbital velocity of the Sun ($V_{\text{rot}} = 220$ km s $^{-1}$), (Bovy, 2015; Eilers et al., 2019; Poder et al., 2023). Furthermore, the height of the Sun above the Galactic plane is estimated to be $Z_0 = 25 \pm 5$ pc (Juric et al., 2008).

The equatorial coordinates (α , δ), distance (d), and mean proper motion components ($\mu_\alpha \cos \delta$, μ_δ) derived in Section 4, along with the radial velocity obtained from Hunt & Reffert (2023), were used in this analysis. To estimate the current positions of King 2 and King 5, the clusters orbits were traced forward in time using integration steps of 1 Myr up to their respective ages. The orbit integration yielded the following results for King 2: apogalactic distance ($R_a = 13.076 \pm 1.555$ kpc), perigalactic distance ($R_p = 7.379 \pm 2.024$ kpc), eccentricity ($e = 0.279 \pm 0.063$); for King 5 apogalactic distance ($R_a = 10.302 \pm 0.115$ kpc), perigalactic distance ($R_p = 9.717 \pm 0.174$ kpc) and eccentricity ($e = 0.06 \pm 0.008$). All orbital parameters are listed in Table 8.

The maximum height reached by King 2 and King 5 above the Galactic plane (Z_{max}) is measured as 499 ± 25 pc and 177 ± 2 pc, respectively. This suggests that both clusters are part of the Milky Way's young stellar disc component (Guctekin et al., 2019). Figure 11 bottom shows the 3D trajectory of the clusters around the Galactic

^{††}<https://galpy.readthedocs.io/en/v1.5.0/>

center. As shown, both King 2 and King 5 follow nearly circular orbits while gradually moving away from the Galactic plane during their revolutions. Moreover, Figure 11 (top) illustrates the evolution of the clusters' distances on the $R_{\text{gc}} \times t$ plane over time. This representation highlights how uncertainties in the initial conditions influence the orbital paths of the clusters.

8. Conclusion

In this work, we carried out a comprehensive photometric and kinematical study of the old OCs King 2 and King 5, providing a significant contribution to their characterization by employing an extensive dataset from *Gaia* DR3, involving a total of 340 member candidates for King 2 and 403 for King 5, with membership probabilities of $P_{\text{ASteCA}} \geq 50\%$. Using the ASTECA package, we estimated spatial structures through radial density profiles, verified membership probabilities, and conducted isochrone fitting to determine reddening, distance modulus, metallicity, age, and other astrophysical parameters. Based on the derived luminosity functions and adopted isochrones (Bressan et al., 2012), the masses of King 2 and King 5 were calculated as $356 \pm 19 M_{\odot}$ and $484 \pm 22 M_{\odot}$, respectively, with mass function slopes (α) of -2.62 ± 0.02 and -2.08 ± 0.01 , consistent with Salpeter (1955). Kinematic analysis indicated the apex positions as $(-142^{\circ}.61 \pm 0^{\circ}.08, -63^{\circ}.58 \pm 0^{\circ}.13)$ for King 2 and $(-115^{\circ}.10 \pm 0^{\circ}.09, -73^{\circ}.16 \pm 0^{\circ}.12)$ for King 5. The ages and distances were determined to be 4.80 ± 0.30 Gyr and 1.45 ± 0.10 Gyr, and 6586 ± 164 pc and 2220 ± 40 pc, respectively, with metallicity values of $[Fe/H] = -0.25$ dex ($z = 0.0088$) for King 2 and $[Fe/H] = -0.15$ dex ($z = 0.0109$) for King 5. Furthermore, we identified 17 and 4 blue straggler stars (BSSs) in King 2 and King 5, respectively, suggesting varied evolutionary processes. Solar elements and dynamical relaxation parameters ($\tau \gg 1$) confirmed that both clusters are dynamically relaxed with 3D morphologies elongated within the Galactic disc. Orbital analysis using the MW^{POTENTIAL}2014 model in GALPY (Bovy, 2015) revealed apogalactic distances of 13.076 ± 1.555 kpc and 10.302 ± 0.115 kpc, perigalactic distances of 7.379 ± 2.024 kpc and 9.132 ± 0.232 kpc, eccentricities of 0.279 and 0.06, and maximum heights of 499 ± 25 pc and 177 ± 2 pc, firmly placing them within the young stellar disc.

Acknowledgments

We express our gratitude to the anonymous referee for their valuable comments and suggestions, which are very helpful in improving our manuscript. This study presents results derived from the European Space Agency (ESA) space mission *Gaia*. The data from *Gaia* are processed by the *Gaia* Data Processing and Analysis Consortium (DPAC). Financial support for DPAC is provided by national institutions, primarily those participating in the *Gaia* Multi-Lateral Agreement (MLA). For additional information, the official *Gaia* mission website can be accessed at <https://www.cosmos.esa.int/gaia>, and the *Gaia* archive is available at <https://archives.esac.esa.int/gaia>.

The author would like to express their gratitude to the Deanship of Scientific Research at Northern Border University, Arar, KSA, for funding this research under project number "NBU-FFR-2025-237-04".

Data availability statement

All data that support the findings of this study are included within the article (and any supplementary files).

Declarations

The authors declare that they have no known competing financial interests or personal relationships that could have appeared to influence the work reported in this paper.

Ethical approval

Not Applicable.

ORCiD

- A. A. Haroon: <https://orcid.org/0000-0002-8194-5836>
- W. H. Elsanhoury: <https://orcid.org/0000-0002-2298-4026>
- Essam Elkholy: <https://orcid.org/0000-0002-1936-9188>
- A. S. Saad: <https://orcid.org/0000-0002-5145-645X>
- Deniz Cennet Cinar: <https://orcid.org/0000-0001-7940-3731>

References

Aparicio, A., Bertelli, G., Chiosi, C., and Garcia-Pelayo, J.M. 1990, *Astrophysics and Space Science*, **169**(1-2), 37. doi:10.1007/BF00640682.

Alvarez Baena, N., Carrera, R., Thompson, H., Balaguer Nunez, L., Bragaglia, A., Jordi, C., Silva-Villa, E., and Vallenari, A.: 2024, *Astronomy and Astrophysics* **687**, A101. doi:10.1051/0004-6361/202348220.

Alfonso, J., Vieira, K., and Garcia-Varela, A.: 2024, *arXiv e-prints*, arXiv:2410.23527. doi:10.48550/arXiv.2410.23527.

Antonini, F., Chatterjee, S., Rodriguez, C.L., Morscher, M., Pattabiraman, B., Kalogera, V., and, ...: 2016, *The Astrophysical Journal* **816**, 65. doi:10.3847/0004-637X/816/2/65.

Arnold, A.D. and Baumgardt, H.: 2025, *Monthly Notices of the Royal Astronomical Society* **537**, 1807. doi:10.1093/mnras/staf121.

Bhattacharya, S., Rao, K.K., Agarwal, M., Balan, S., and Vaidya, K.: 2022, *Monthly Notices of the Royal Astronomical Society* **517**, 3525. doi:10.1093/mnras/stac2906.

Bisht, D., Elsanhoury, W. H., Zhu, Q., Sariya, D. P., Yadav, R. K. S., Rangwal, G., Durgapal, A., and Jiang, I.: 2020, *The Astronomical Journal*, **160**(3), 119. doi:10.3847/1538-3881/ab9ffd, arXiv:2006.13618.

Bisht, D., Yadav, R.K.S., Ganesh, S., Durgapal, A.K., Rangwal, G., and Fynbo, J.P.U.: 2019, *Monthly Notices of the Royal Astronomical Society*, **482**(2), 1471. doi:10.1093/mnras/sty2781, arXiv:1810.05380.

Bisht, D., Zhu, Q., Yadav, R.K.S., Rangwal, G., Sariya, D.P., Durgapal, A., and Jiang, I: 2022, *Publications of the Astronomical Society of the Pacific*, **134**(1034), 044201.

Bland-Hawthorn, J., Sharma, S., Tepper-Garcia, T., Binney, J., Freeman, K. C., Hayden, M. R., Kos, J., De Silva, G. M., Ellis, S., Lewis, G. F., Asplund, M., Buder, S., Casey, A. R., D’Orazi, V., Duong, L., Khanna, S., Lin, J., Lind, K., Martell, S. L., Ness, M. K., Simpson, J. D., Zucker, D. B., Zwitter, T., Kafle, P. R., Quillen, A. C., Ting, Y., Wyse, R. F. G.: 2019, *Monthly Notices of the Royal Astronomical Society*, **486**(1), 1167. doi:10.1093/mnras/stz217, arXiv:1809.02658.

Bossini, D., Vallenari, A., Bragaglia, A., Cantat-Gaudin, T., Sordo, R., Balaguer-Núñez, L.: 2019, *Astronomy and Astrophysics* **623**, A108. doi:10.1051/0004-6361/201834693.

Bonatto, C. & Bica, E. 2009, *Monthly Notices of the Royal Astronomical Society*, **397**(4), 1915. doi:10.1111/j.1365-2966.2009.14877.x, arXiv:0904.1321.

Bovy, J. 2015, *The Astrophysical Journal*, **216**(2), 29. doi:10.1088/0067-0049/216/2/29, arXiv:1412.3451.

Baumgardt, H., Faller, J., Meinholt, N., McGovern-Greco, C., and Hilker, M.: 2022, *Monthly Notices of the Royal Astronomical Society* **510**, 3531. doi:10.1093/mnras/stab3629.

Bressan, A., Marigo, P., Girardi, L., Salasnich, B., Dal Cero, C., Rubele, S., Nanni, A.: 2012, *Monthly Notices of the Royal Astronomical Society*, **427**(1), 127. doi:10.1111/j.1365-2966.2012.21948.x, arXiv:1208.4498.

Bukowiecki, L., Maciejewski, G., Konorski, P., and Strobel, A.: 2011, *Acta Astronomica*, **61**(3), 231. doi:10.48550/arXiv.1107.5119, arXiv:1107.5119.

Cabrera-Cano, J. & Alfaro, E. J. 1990, *Astronomy and Astrophysics*, **235**, 94.

El Aziz, M.A., Selim, I.M., and Essam, A.: 2016, *Experimental Astronomy* **42**, 49. doi:10.1007/s10686-016-9499-9.

Cantat-Gaudin, T., Jordi, C., Vallenari, A., Bragaglia, A., Balaguer-Núñez, L., Soubiran, C., Bossini, D., Moitinho, A., Castro-Ginard, A., Krone-Martins, A., Casamiquela, L., Sordo, R., Carrera, R. : 2018, *Astronomy and Astrophysics*, **618**, A93. doi:10.1051/0004-6361/201833476, arXiv:1805.08726.

Cantat-Gaudin, T., Anders, F., Castro-Ginard, A., Jordi, C., Romero-Gómez, M., Soubiran, C., Casamiquela, L., Tarricq, Y., Moitinho, A., Vallenari, A., Bragaglia, A., Krone-Martins, A., and Kounkel, M.: 2020, *Astronomy & Astrophysics*, **640**, A1. doi:10.1051/0004-6361/202038192, arXiv:2004.14376.

Capitanio, L., Lallement, R., Vergely, J. L., Elyajouri, M., and Monreal-Ibero, A.: 2017, *Astronomy and Astrophysics*, **606**, A65. doi:10.1051/0004-6361/201730831, arXiv:1706.07711.

Carraro, G. & Vallenari, A. 2000, *Astronomy and Astrophysics*, **142**, 59. doi:10.1051/aas:2000137, arXiv:astro-ph/9911410.

Casagrande, L. & VandenBerg, D. A. 2018, *Monthly Notices of the Royal Astronomical Society*, **479**(1), L102. doi:10.1093/mnrasl/sly104, arXiv:1806.01953.

Chand, K., Rao, K.K., Vaidya, K., and Panthi, A.: 2024, *The Astronomical Journal* **168**, 278. doi:10.3847/1538-3881/ad85d2

Chupina N. V., Reva V. G., Vereshchagin S. V., 2001, *A&A*, **371**, 115. doi:10.1051/0004-6361:20010337.

Çakmak, H., Yontan, T., Bilir, S., Banks, T. S., Michel, R., Soydugan, E., Koc, S., and Ercay, H.: 2024, *AN*, 345, e20240054. doi:10.1002/asna.20240054.

Dias W. S., Alessi B. S., Moitinho A., Lépine J. R. D., 2002, *A&A*, **389**, 871. doi:10.1051/0004-6361:20020668.

Dib S., Basu S., 2018, *A&A*, **614**, A43. doi:10.1051/0004-6361/201732490.

Durgapal, A. K., Pandey, A. K., & Mohan, V. 1998, *Bulletin of the Astronomical Society of India*, **26**, 551.

Dursun, D. C., Taşdemir, S., Koc, S., and Iyer, S.: 2024, *Physics and Astronomy Reports*, **2**(1), 1-17. doi:10.26650/PAR.2024.00002, arXiv:2404.13115.

Eilers, A.C., Hogg, D.W., Rix, H.-W., and Ness, M.K.: 2019, *The Astrophysical Journal* **871**, 120. doi:10.3847/1538-4357/aaf648.

Elsanhouri, W. H. 2021, *Journal of Astrophysics and Astronomy*, **42**(2), 90. doi:10.1007/s12036-021-

09771-x, arXiv:2103.13603.

Elsanhouri, W. H., Amin, M. Y., Haroon, A. A. and Awad, Z.: 2022, *Journal of Astrophysics and Astronomy*, **43**(1), 26. doi:10.1007/s12036-022-09810-1, arXiv:2201.04015.

Elsanhouri, W. H., Haroon, A. A., Elkholly, E. A., and Çınar, D. C. 2024, *arXiv e-prints*, doi:10.48550/arXiv.2412.07871, arXiv:2412.07871.

Elsanhouri, W. H., Bisht, D., Belwal, K., Haroon, A. A., Elkholly, E. A., Sariya, D. P., and, Bisht, M. S., and Raj, A.: 2025, *Advances in Space Research* **75**, 1502. doi:10.1016/j.asr.2024.11.004.

Friel, E. D. 1995, *Annual Review of Astronomy and Astrophysics*, **33**, 381. doi:10.1146/annurev.aa.33.090195.002121.

Fujii, M.S. and Portegies Zwart, S.: 2016, *The Astrophysical Journal* **817**, 4. doi:10.3847/0004-637X/817/1/4.

Gaia Collaboration, Brown, A. G. A., Vallenari, A. .: 2018, *Astronomy and Astrophysics*, **616**, A1. doi:10.1051/0004-6361/201833051, arXiv:1804.09365.

Gaia Collaboration, Brown, A.G.A., Vallenari, A., Prusti, T., de Bruijne, .: 2021, *Astronomy and Astrophysics* **649**, A1. doi:10.1051/0004-6361/202039657.

Gaia Collaboration, Vallenari, A., Brown, A. G. A. .: 2023, *Astronomy and Astrophysics*, **674**, A1. doi:10.1051/0004-6361/202243940, arXiv:2208.00211.

Gosnell, N.M., Mathieu, R.D., Geller, A.M., Sills, A., Leigh, N., and Knigge, C.: 2015, *The Astrophysical Journal* **814**, 163. doi:10.1088/0004-637X/814/2/163.

Guctekin, S. T., Bilir, S., Karaali, S., Plevne, O., and & Ak, S.: 2019, *Advances in Space Research*, **63**, 1360-1373. doi:10.1016/j.asr.2018.10.041

Gustafsson, B., Church, R. P., Davies, M. B. and Rickman, H.: 2016, *Astronomy and Astrophysics*, **593**, A85. doi:10.1051/0004-6361/201423916, arXiv:1605.02965.

Haroon, A. A., Elsanhouri, W. H., Saad, A. S. and Elkholly, E. A.: 2024, *Contributions of the Astronomical Observatory Skalnate Pleso*, **54**(3), 22. doi:10.31577/caosp.2024.54.3.22.

Hunt, E. L. & Reffert, S. 2023, *Astronomy and Astrophysics*, **673**, A114. doi:10.1051/0004-6361/202346285, arXiv:2303.13424.

Hunt, J.A.S. and Vasiliev, E.: 2025, *arXiv e-prints*, arXiv:2501.04075. doi:10.48550/arXiv.2501.04075.

Ishchenko M., Masliukh V., Hradov M., Berczik P., Shukirgaliyev B., Omarov C., 2025, *Astronomy and Astrophysics*, **694**, A33. doi:10.1051/0004-6361/202452336

Jadhav, V.V., Pandey, S., Subramaniam, A., and Sagar, R.: 2021, *Journal of Astrophysics and Astronomy* **42**, 89. doi:10.1007/s12036-021-09746-y.

Jadhav, V. V., Pennock, C. M., Subramaniam, A. Sagar, R., and Nayak, R. K.: 2021, *Monthly Notices of the Royal Astronomical Society*, **503**(1), 236. doi:10.1093/mnras/stab213, arXiv:2101.07122.

Joshi, Y. C., Maurya, J., John, A. A., Panchal, A., Joshi, S. and Kumar, B.: 2020, *Monthly Notices of the Royal Astronomical Society*, **492**(3), 3602. doi:10.1093/mnras/staa029, arXiv:2001.04068.

Joshi, Y.C., Deepak, and Malhotra, S.: 2024, *Frontiers in Astronomy and Space Sciences* **11**, 1348321. doi:10.3389/fspas.2024.1348321.

Jurić, M., Ivezić, Ž., Brooks, A. Lupton, R. H., Schlegel, D., Finkbeiner, D., Padmanabhan, N.: 2008, *The Astrophysical Journal*, **673**(2), 864. doi:10.1086/523619, arXiv:astro-ph/0510520.

Kafle, P.R., Sharma, S., Lewis, G.F., Robotham, A.S.G., and Driver, S.P.: 2018, *Monthly Notices of the Royal Astronomical Society* **475**, 4043. doi:10.1093/mnras/sty082.

Kaluzny, J. 1989b, *Acta Astronomica*, **39**, 13.

King, I. 1962, *The Astronomical Journal*, **67**, 471. doi:10.1086/108756.

Kroupa, P. 2002, *Science*, **295**(5552), 82. doi:10.1126/science.1067524, arXiv:astro-ph/0201098.

Küpper, A.H.W., Balbinot, E., Bonaca, A., Johnston, K.V., Hogg, D.W., Kroupa, P.: 2015, *The Astrophysical Journal* **803**, 80. doi:10.1088/0004-637X/803/2/80.

Lada, C. J. & Lada, E. A. 2003, *Annual Review of Astronomy and Astrophysics*, **41**, 57. doi:10.1146/annurev.astro.41.011802.094844, arXiv:astro-ph/0301540.

Leiner, E.M. and Geller, A.: 2021, *The Astrophysical Journal* **908**, 229. doi:10.3847/1538-4357/abd7e9.

Liu, X., He, Z., Luo, Y., and Wang, K.: 2025, *Monthly Notices of the Royal Astronomical Society* **537**,

2403. doi:10.1093/mnras/staf153.

Nilakshi, Sagar, R., Pandey, A. K., and Mohan, V.: 2002, *Astronomy and Astrophysics*, **383**, 153. doi:10.1051/0004-6361:20011719.

Pang, X., Yu, Z., Tang, S.-Y., Jongsuk, H., Yuan, Z., Mario, P., and Kouwenhoven, M. B. N.: 2021, *The Astronomical Journal*, **923**, 20. doi:10.3847/1538-4357/ac2838, arXiv:2106.07658.

Perren, G. I., Vázquez, R. A., & Piatti, A. E. 2015, *Astronomy and Astrophysics*, **576**, A6. doi:10.1051/0004-6361/201424946, arXiv:1412.2366.

Pera, M.S., Perrén, G.I., Navone, H.D., and Vázquez, R.A.: 2024, *Boletin de la Asociacion Argentina de Astronomia La Plata Argentina* **65**, 94.

Peterson, C. J. & King, I. R. 1975, *The Astronomical Journal*, **80**, 427. doi:10.1086/111759.

Pöder, S., Benito, M., Pata, J., Kipper, R., Ramler, H., Hütsi, G., and, ...: 2023, *Astronomy and Astrophysics* **676**, A134. doi:10.1051/0004-6361/202346474.

Phelps, R. L., Janes, K. A., & Montgomery, K. A. 1994, *The Astronomical Journal*, **107**, 1079. doi:10.1086/116920.

Piatti, A. E. 2016, *Monthly Notices of the Royal Astronomical Society*, **463**(4), 3476. doi:10.1093/mnras/stw2248, arXiv:1609.01209.

Piatti, A. E., Bica, E., Santos, J. F. C., and Claria, J. J.: 2002, *Astronomy and Astrophysics*, **387**, 108. doi:10.1051/0004-6361:20020373.

Qin, C., Pang, X., Pasquato, M., Kouwenhoven, M.B.N., and Vallenari, A.: 2024, *arXiv e-prints*, arXiv:2412.08710. doi:10.48550/arXiv.2412.08710.

Rain, M. J., Ahumada, J. A., and Carraro, G.: 2021, *Astronomy and Astrophysics*, **650**, A67. doi:10.1051/0004-6361/202040072.

Rangwal, G., Yadav, R. K. S., Durgapal, Bisht, D., Nardiello, D.: 2019, *Monthly Notices of the Royal Astronomical Society*, **490**(1), 1383. doi:10.1093/mnras/stz2642, arXiv:1909.08810.

Riello, M., De Angelis, F., Evans, D. W. ...: 2021, *Astronomy and Astrophysics*, **649**, A3. doi:10.1051/0004-6361/202039587, arXiv:2012.01916.

Röser, Siegfried and Schilbach, Elena. 2019, *Astronomy and Astrophysics*, **627**, A4. doi:10.1051/0004-6361/201935502, arXiv:1903.08610.

Salpeter, E. E. 1955, *The Astrophysical Journal*, **121**, 161. doi:10.1086/145971.

Soubiran C., Cantat-Gaudin T., Romero-Gomez M. Casamiquela, L., Jordi, C., Vallenari, A., Antoja, T., Balaguer-Núñez, L., Bossini, D., Bragaglia, A., Carrera, R., Castro-Ginard, A., Figueras, F., Heiter, U., Katz, D., Krone-Martins, A., Le Campion, J. -F., Moitinho, A., Sordo, R.: 2018, *A&Ap*, **619**, 155. doi:10.1051/0004-6361/201834020.

Scott, D. W. 1992, *Multivariate Density Estimation*.

Sindhu, N., Subramaniam, A., Jadhav, V.V., Chatterjee, S., Geller, A.M., Knigge, C., and, ...: 2019, *The Astrophysical Journal* **882**, 43. doi:10.3847/1538-4357/ab31a8.

Spitzer, J. L. & Hart, M. H. 1971, *The Astrophysical Journal*, **164**, 399. doi:10.1086/150855.

Taşdemir, S. & Yontan, T. 2023, *Physics and Astronomy Reports*, **1**(1), 1. doi:10.26650/PAR.2023.00001, arXiv:2304.14270.

Taşdemir, S. & Çınar, D.C.: 2025, *arXiv e-prints*, arXiv:2501.17235. doi:10.48550/arXiv.2501.17235.

Sableviciute, I., Vansevicius, V., Kodaira, K. Narbutis, D., Stonkute, R., Bridzius, A.: 2006, *Baltic Astronomy*, **15**, 547. doi:10.48550/arXiv.astro-ph/0701774, arXiv:astro-ph/0701774.

Warren, S. R. & Cole, A. A. 2009, *Monthly Notices of the Royal Astronomical Society*, **393**(1), 272. doi:10.1111/j.1365-2966.2008.14268.x, arXiv:0811.2925.

Yontan, T., Cakmak, T., Bilir, S. Banks, T., Raul, M., Canbay, R., Koc, S., Tasdemir, S., Erçay, H., Tanik-Ozturk, B., Dursun, D. C.: 2022, *Revista Mexicana de Astronomía y Astrofísica*, **58**, 333. doi:10.22201/ia.01851101p.2022.58.02.14, arXiv:2207.06407.

Yontan, T., Canbay, R., 2023, *Physics and Astronomy Reports* **1**, 65. doi:10.26650/PAR.2023.00008.

Yontan, T. 2023, *The Astronomical Journal*, **165**(3), 79. doi:10.3847/1538-3881/aca6f0.

Yucel, G., Canbay, R., & Bakis, V. 2024, *Physics and Astronomy Reports*, **2**(1), 18. doi:10.26650/PAR.2024.00003, arXiv:2404.18171.

Zeidler, P., Nota, A., Grebel, E. K. Sabbi, E., Pasquali, A., Tosi, M., Christian, C.: 2017, *The Astronomical Journal*, **153**(3), 122. doi:10.3847/1538-3881/153/3/122, arXiv:1701.07302.

Zhong, J., Chen, L., Kouwenhoven, M. B. N., Li, L., and Shao, Z.: 2019, *Astronomy and Astrophysics*, **624**, A34. doi:10.1051/0004-6361/201834334, arXiv:1902.06892.